NONLINEAR TIME-FREQUENCY CONTROL OF A HIGH-SPEED SPINDLE USING ACTIVE MAGNETIC BEARINGS

A Thesis

by

JACOB DANIEL SOUTHERN

Submitted to the Office of Graduate and Professional Studies of
Texas A&M University
in partial fulfillment of the requirements for the degree of

MASTER OF SCIENCE

Chair of Committee,	C. Steve Suh
Committee Members,	Wayne Nguyen Hung
	Pilwon Hur
Head of Department,	Andreas Polycarpou

May 2017

Major Subject: Mechanical Engineering

ABSTRACT

The objective of this research was to demonstrate the capability of a novel design of a high-speed spindle using combination active magnetic bearings (AMBs) with a nonlinear time-frequency controller. The spindle modeled for this research was a five degree of freedom system with a fixed constant rotational velocity in the z-direction of 192,000 RPMs. The spindle was also considered a flexible shaft with static and dynamic eccentricities. The AMBs used in this research were a homopolar design that included both the radial and thrust components in one AMB. These AMBs also used permanent magnets to levitate the system. One combination AMB, along with another radial AMB, was used to support the system.

The controller algorithm was based on discrete wavelet transformations (DWT) and filtered-x least-mean-square (FXLMS) algorithm. The logic of this controller implements DWT and FXLMS adaptive filters to perform a feedforward control, online identification and to construct parallel adaptive filter banks. The use of DWT allows the controller to simultaneously control time and frequency of the system, and the transformation between the two domains is a lossless transformation.

For test purposes the controller was brought online at the same time the system was turned on. Once the system was under control an impulse force of 250 kN was applied to the system to see if the controller was capable of bringing the system back under control. The controller demonstrated control in both the time and frequency domain. The controlled system had a maximum controlled displacement of 2.85×10^{-5} meters with an allowable displacement of 0.55×10^{-3} meters. In the frequency domain,

instantaneous frequency shown using the Hilbert-Huang Transformation (HHT) was used. The frequency response was a highly nonlinear broadband response that was brought under control, and the frequency bandwidth was reduced to a quasiperiodic and predictable response. The bandwidth of the system was reduced to 1.5% of the original bandwidth.

Overall this high-speed spindle design demonstrated the capability of running and being controlled at a speed of 192,000 RPMs. The next step is to validate the controller and AMBs using a physical system.

ACKNOWLEDGEMENTS

I would like to thank my committee chair, Dr. Suh, and my committee members, Dr. Hur and Dr. Hung, for their guidance and support throughout the course of this research.

Thanks also go to my friends and colleagues and the department faculty and staff for making my time at Texas A&M University a great experience.

Finally, thanks to my mother and father for their encouragement and to my wife for her patience and love.

CONTRIBUTORS AND FUNDING SOURCES

This work was supervised by a thesis committee consisting of Professors C. Steve Suh and Pilwon Hur of the Department of Mechanical Engineering and Professor Wayne Nguyen Hung of the Department of Engineering Technology and Industrial Distribution. All work for the thesis was completed independently by the student without outside financial support.

TABLE OF CONTENTS

Page

LIST OF FIGURES

Page

LIST OF TABLES

Page

1. INTRODUCTION

1.1 Overview

The world is relentlessly striving to build devices that are faster and smaller than their previous versions. This effort poses problems of how to create and control these new devices. This paper will focus on high-speed spindles and how to control them using new methods. These spindles are located in a range of different devices. Some examples of these devices are lathes, mills, turbines and windmills. The spindle is the most important part of these devices because this part translates the rotational input from the motor. In a lathe the spindle is what transfers the rotational energy to the work piece so cutting may occur. An example of a lathe spindle can be seen below in Figure 1.

Figure 1: Lathe Headstock Spindle [1]

All of these devices have limited operational speed due to limitations of the control system and the mechanical bearings used in these systems. Some of the main issues with these systems are the increased amounts of friction, vibration and heat generated during

higher operational speeds. This research is done to prove the capability of a new spindle-AMBs design configuration that has the potential to eliminate some of these main issues. With these issues eliminated the systems could be redesigned for the optimal size, weight and speed.

1.2 Active Magnetic Bearings

The component responsible for most of the issues with spindles is the mechanical bearings. This research uses active magnetic bearings (AMBs) to reduce the effects of these issues. The concept of using magnets to levitate an object freely dates back as early as 1842 with Samuel Earnshaw's experiments [2]. It was not until recently that this concept became a viable option with the use of AMBs and the switch from analog to digital controllers. The two main types of AMBs are radial and thrust bearings. An example of a radial and thrust AMB assembly can be seen below in Figure 2.

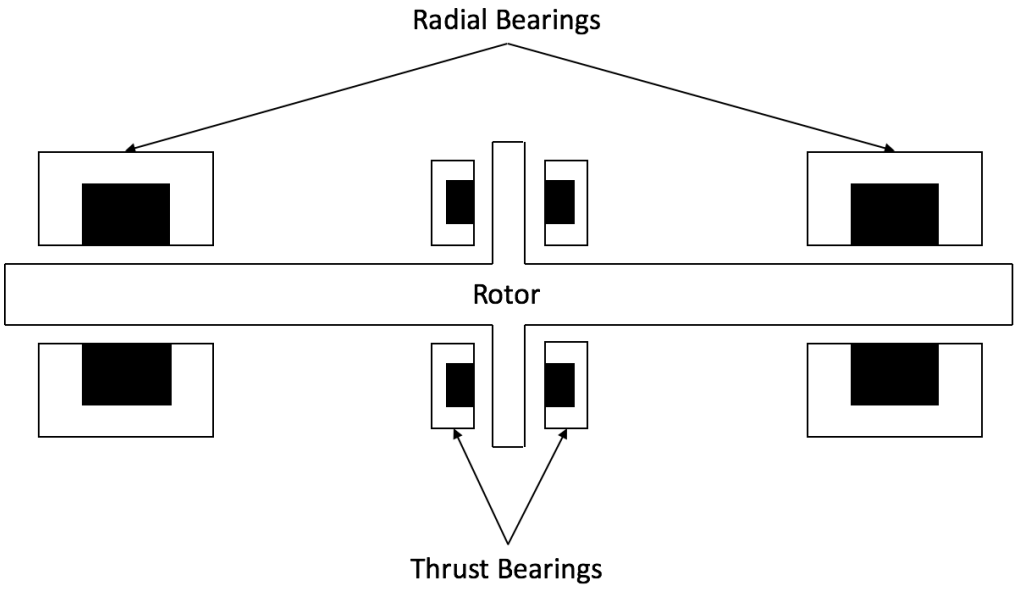

Figure 2: Radial and Thrust AMBs

The AMBs use an electromagnetic force, *f*, to levitate an object and the equation for the force is given by:

$$f = \frac{B^2 A_g}{\mu_0} \tag{1.1}$$

The electromagnetic flux density, B, is the amount of electromagnetic flux per unit area:

$$B = \frac{\phi}{A_g} \tag{1.2}$$

where, ϕ, is the electromagnetic flux, A_g, is the area of the coil and, μ_0, is the permeability of the free space [3]. The field traveling from the north pole to the south pole creates this electromagnetic field. An example of this is presented in Figure 3.

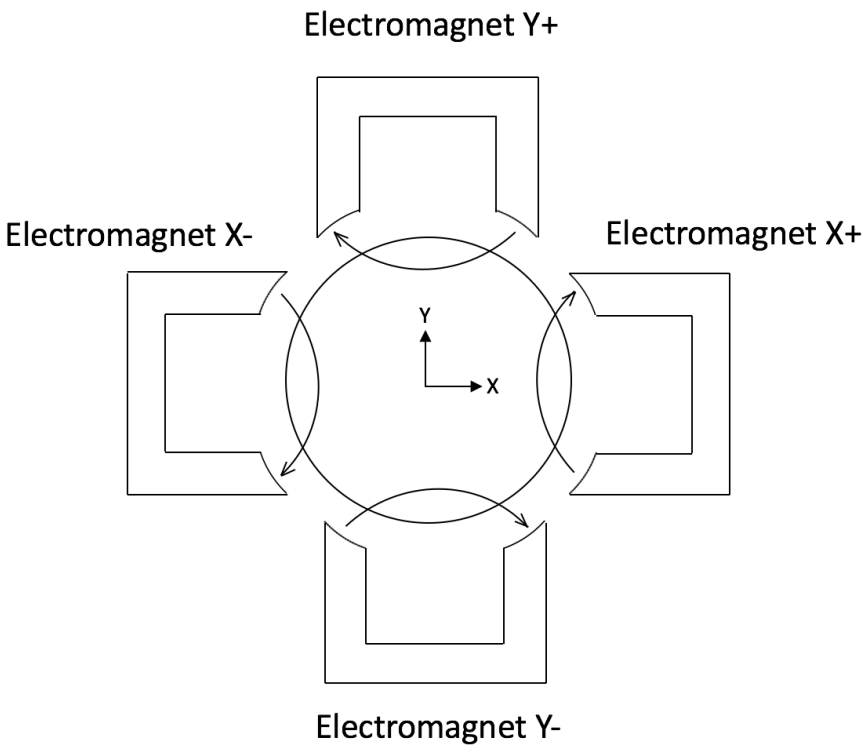

Figure 3: Magnetic Field Lines

The rotation of the object through the non-uniform electromagnetic field causes eddy currents and leads to a skin effect. This skin effect is a thin layer that holds the electromagnetic force from the AMBs because the eddy currents cause the electromagnetic field to be expelled from the rotor. The thinner this layer is the less efficient the AMB will be. The thickness of this layer is calculated using the equation below:

$$\delta = \sqrt{\frac{1}{\pi \mu_0 \mu \sigma f_e}} \tag{1.3}$$

where μ and σ are the permeability and conductivity of the object and f_e is the electrical frequency which is based on the rotor rotational frequency and the pole orientation of the AMB [4]. The best way to increase the thickness of this skin layer and reduce the effects of eddy currents is to laminate the material [5]. This works by blocking the eddy currents from disrupting and expelling the electromagnetic field.

A sensor that constantly measures the air gap distance, a control scheme, and a power amplifier are needed to control the position of the spindle in the AMB. A basic schematic of the AMB and the components needed is shown below in Figure 4.

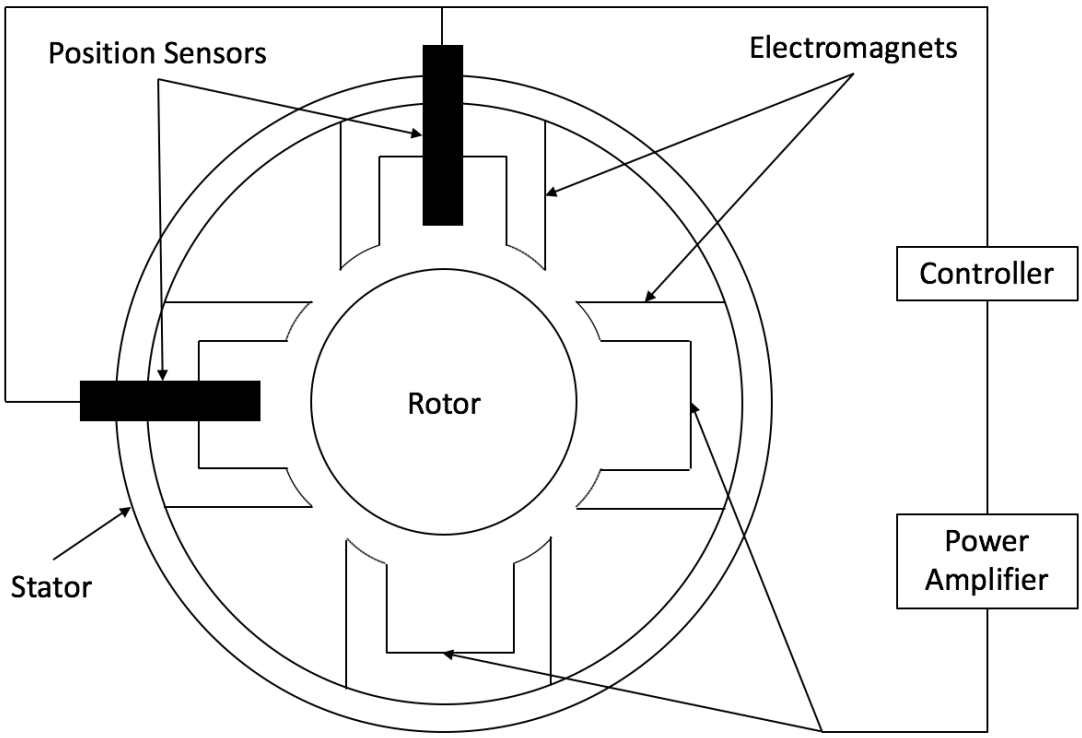

Figure 4: AMB and Basic Components

With the traditional AMB design a current is constantly required to keep the spindle from contacting the AMB. This current is called the bias current and is used to levitate the spindle. The limitation of this bearing design requires the AMB to always be powered. Because these AMBs require a bias current they also have a backup mechanical bearing in case the system was to lose power. These backup mechanical bearings are used to protect the AMB from any contact with the spindle. The backup bearings limit the operational speed of the system because they need to be able to handle the operational speed if any contact were to occur.

The AMBs used in this research is a combination design. This design encompasses a radial and thrust bearing in one AMB. With this design, the number of

AMBs needed to control the system is reduced. This reduction of AMBs will also contribute to a reduction of size and weight of the system. A conventional three AMB system can be seen below in Figure 5.

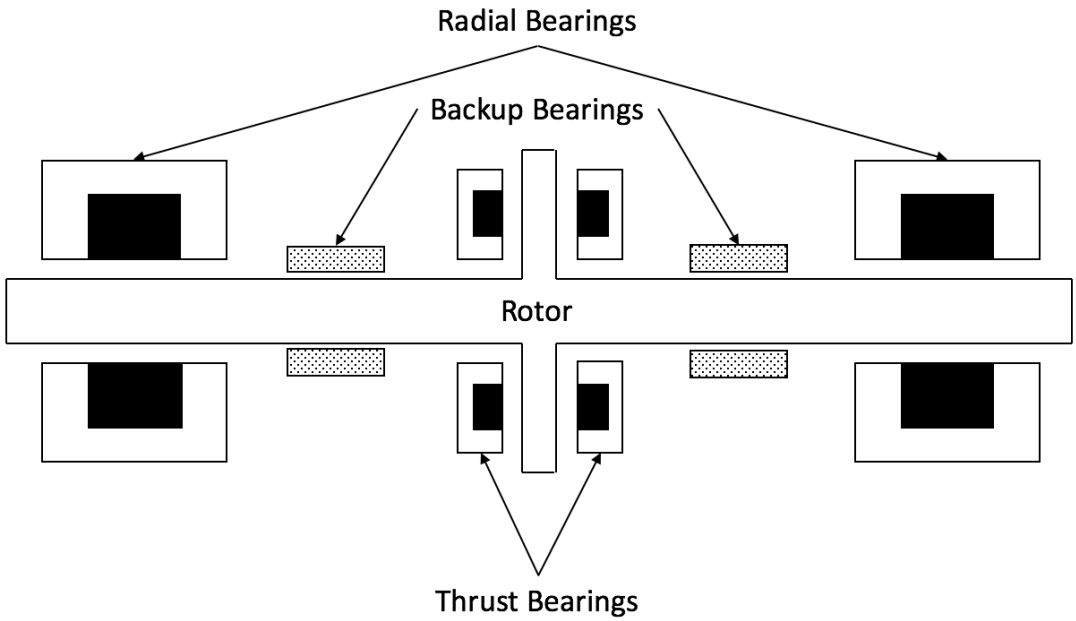

Figure 5: Conventional Three AMB System

With the combination design AMB, the same system can be reduced to two AMBs. An example of the combination two AMB system can be seen below in Figure 6.

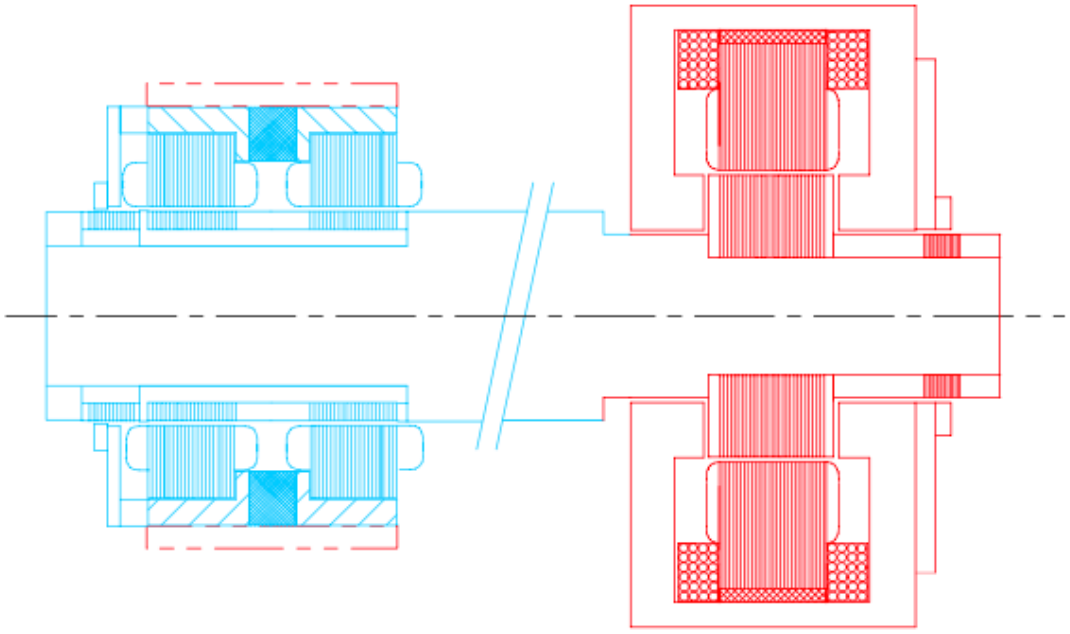

Figure 6: Combination Two AMB System [6]

Some of the other benefits to these combination bearings is the construction in a homopolar configuration. This allows the bias field to be of one polarity on the radials and the opposite polarity on the axial poles [6]. This design eliminates the field polarity changes in the radial direction and will minimize eddy current effects [6]. This combination design does not require a bias current because the AMBs use permanent magnets to initially levitate the spindle [6]. An example of the combination bearing design can be seen below in Figure 7.

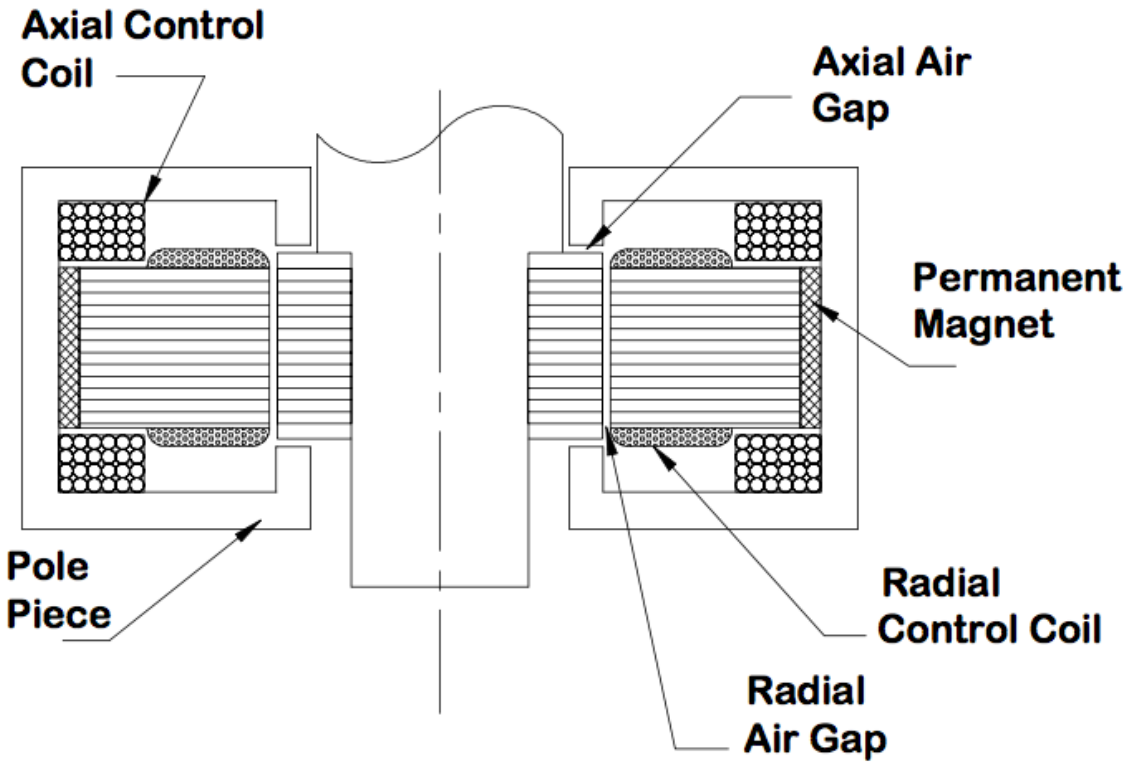

Figure 7: Combination Bearing Layout [6]

With the use of permanent magnets, the spindle does not need backup mechanical bearings because if power is lost to the system the permanent magnets will keep the spindle from contacting the AMB. The removal of the backup mechanical bearings will allow the system to reach speeds that are not currently reachable. Another benefit of these combination AMBs is no cross-coupling in the design [6]. Neither the radial direction nor the axial direction has any cross-coupling during the operation of these AMBs. This lack of cross coupling has been verified in real world models [6]. The lack of cross coupling allows for easier control and modeling of the AMBs. With these AMBs, the system will be smaller and lighter than a system with conventional AMBs.

1.3 Issues of Present Work

The current machining spindle is designed with the mitigation of vibration as the primary driving factor. Spindle designs accomplish this by making the system very stiff with the help of mechanical bearings and increasing mass. A downside to this design is the stiffness and damping coefficients are not adjustable and a special foundation is required to mount these machines. This foundation helps to isolate the system from outside vibrations. Also, the mechanical bearings limit the operation speed of the machine because their damping coefficient is a set parameter that cannot be adjusted for varying speeds. This is a rudimentary approach to the problem of vibrations in a spindle. The best way to remove vibrations is to completely isolate the spindle from the system and have the ability to adjust the stiffness and damping coefficients. This is possible with AMBs because the spindle will be suspended using magnetic force, thus removing vibrations in the spindle caused by the contact of the machine. The only vibration remaining is caused by the imbalance in the spindle, which can be mitigated using a robust controller for the AMBs.

AMBs have been a highly-researched topic lately for their benefits of controlling rotating objects. A combination of radial and axial AMBs allows the system to control five degrees-of-freedom. With the use of AMBs, the systems mass can be greatly reduced because it will no longer be needed for vibration mitigation. Also, the decrease in mass and adjustable parameters will allow the system to be placed on a normal foundation. The current models for AMBs linearize the governing equations of the spindle, ignore gyroscopic effects in the spindle, and use a linear control method [7]. All

of these issues cause the actual system to not reach high speed operation. When the spindle is linearized and the gyroscopic effects ignored the controller is not capable of controlling a real system. So, when the controller is implanted into a real-world system it is unable to bring the system under control and leads to a failure. For short spindles, ignoring gyroscopic effects would have negligible effects but for this research a long spindle was tested so ignoring gyroscopic effects would be an incorrect assumption. Also, linearizing the spindle governing equations is an incorrect assumption for all spindle lengths when the system is being tested at high speeds. These high speeds cause the system to behave highly nonlinear.

The other major issue is the majority of control schemes for these systems use PID [8]. PID is a linearized control method and does not work at high speeds for these spindle designs because they are highly nonlinear systems. When the system is linearized the controller is developed based on the simplified model. As the physical system cannot be fully characterized by the simplified model, the controller is ineffective in mitigating dynamic instability. This inability to fully characterize the system leads to AMBs being operated at speed below what they are capable of reaching with the correct controller. Most of these control methods only control the system in the time domain. When the time domain error is small, the system could appear to be under control but in the frequency domain the system would still be unstable and can lead to system failure due to high frequency vibrations. This research controls a combination AMB system in the time and frequency domain simultaneously. The control in both domains will ensure that the system is stable and safe to operate at high speeds.

The combination of these factors being corrected will lead to the system having an increased production rate, a decreased power consumption, and the machine will generate less waste when compared to current spindle design.

1.4 Research Objective

The objective of this research is to demonstrate the capability of a design for a high-speed spindle using a Simulink model, which uses AMBs to support the load of the spindle and the excitation forces. This study will allow for the verification of a high-speed spindle design that uses AMBs along with a controller. The design for the AMBs that will be utilized is a combination design of a radial and thrust bearing. A combination design will decrease the amount of AMBs needed to support the spindle and the amount of power required to create the electromagnetic force, compared to having radial and thrust AMBs separately. This design will include a robust controller for the AMBs. The type of controller that will be developed is a wavelet-based nonlinear time-frequency controller. This controller will be extensively tested to validate the superiority of this type of controller. A nonlinear time-frequency controller has already demonstrated the capability of controlling a spindle at 187,500 RPMs with support only in the radial directions [3]. This study however will demonstrate the capability of controlling a five degrees-of-freedom system. After the system is under control an impulse force will be applied in multiple axes to verify that the controller is robust. Upon completion of the research, a numerical and simulink model for a high-speed spindle system will have been created. The following chapters will record the findings of this research. Chapter 2 will present the model for the spindle and the electromagnetic

forces for the AMBs used for the simulations. It will also go over the nonlinear time-frequency controller used during the research. Chapter 3 will represent the results obtained from the simulations and discuss the findings of those results. Chapter 4 will draw conclusions based on the findings of the research and it will present the future work recommended after the findings of this research.

1.5 Research Plan

1. Derive the corresponding dynamic model for a scaled version of a spindle.
2. Find a combination radial-axial AMB design and validate the feasibility of a combination design.
3. Derive the corresponding dynamic model that describes the AMB design.
4. Develop and implement a nonlinear time-frequency controller design based on the derived AMB model.
5. Generate numerical results to validate the AMB model and the controller design.

2. METHOD

The following free body diagram, seen below in Figure 8, is used to create the governing equations of the spindle. The system has one combination AMB at the "A" location and a radial AMB at the "B" location. The x, y and z coordinate system is defined at the center of gravity of the spindle and ψ, θ and ϕ are the rotational directions about those axes, respectively. This is a five degrees-of-freedom system with the rotational speed in the ϕ-direction at a constant velocity.

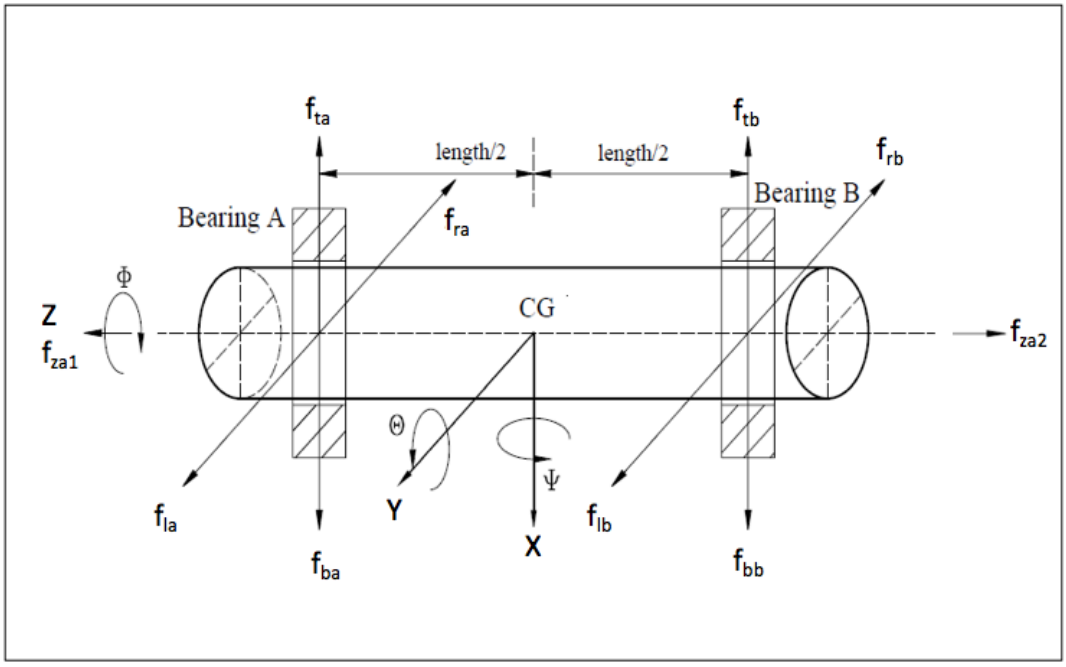

Figure 8: Free Body Diagram of System

2.1 Equations of Motion

The equations of motion for the spindle were derived as a nonlinear set of governing equations in [3]. It was crucial these equations be nonlinear so it was possible

for the controller to demonstrate its robustness. Most research in this area is done with linearized equations. Linearization leads to negating parts of the equations of motion that are crucial for understanding how this high-speed spindle behaves. This research is a nonlinear approach with the inclusion of gyroscopic effects and eccentricities. These effects are considered significant because of the shaft length and the speed at which the system rotates. The shaft is also considered flexible, thus imparting more nonlinearities into the system and allowing for whirling. Whirling occurs when the system reaches a speed that induces violent vibrations in the system. These vibrations can lead to system failure if the system is not controlled properly to mitigate these vibrations. The equations of motion for the spindle can be seen below in Equations 2.1 through 2.5.

$$\ddot{x} = \frac{1}{m_r}(F_{xa} + F_{xb} + F_{xe} + F_i) \tag{2.1}$$

$$\ddot{y} = \frac{1}{m_r}\left(F_{ya} + F_{yb} + F_{ye} - F_i\right) \tag{2.2}$$

$$\ddot{z} = \frac{1}{m_r}(F_{za} + F_i) \tag{2.3}$$

$$\ddot{\theta} = \frac{M_x}{I_r} + \left(\frac{I_p}{I_r}\right)\dot{\phi}\dot{\psi} - \dot{\psi}\sin(\theta) + \left(\frac{I_p}{I_r}\right)\dot{\psi}^2\sin(\theta) \tag{2.4}$$

$$\begin{aligned}\ddot{\psi} = \frac{M_y}{I_r} - \left(\frac{I_p}{I_r}\right)\dot{\phi}\dot{\theta} - \left(\frac{I_p}{I_r}\right)\dot{\psi}\dot{\theta}\sin(\theta) + \dot{\psi}\dot{\theta}\sin(\theta) \\ - \dot{\psi}^2\sin(\theta)\cos(\phi)\left(\sin(\phi) - \cos(\theta)\right)\end{aligned} \tag{2.5}$$

Where F_{xe} and F_{ye} are the forces due to the static and dynamic eccentricity. The F_i is the impulse force that is used to agitate the system after it is under control. The impulse force is used to represent the system being hit by an outside body or the spindle being

used in its normal operations. The impulse force is important for demonstrating the robustness of the controller. This impulse force occurs over a time frame of one thousandth of a second and it is introduced at the center of gravity. The eccentricity forces can be seen below in Equations 2.6 through 2.11.

$$F_{xe} = f_{xd} + f_{\psi d} \tag{2.6}$$

$$F_{ye} = f_{yd} + f_{\theta d} \tag{2.7}$$

$$f_{xd} = m_r \mu \dot{\phi}^2 \sin(\dot{\phi} t) \tag{2.8}$$

$$f_{yd} = m_r \mu \dot{\phi}^2 \cos(\dot{\phi} t) \tag{2.9}$$

$$f_{\psi d} = \frac{2(I_p - I_r)}{L} \tau \dot{\phi}^2 \sin(\dot{\phi} t) \tag{2.10}$$

$$f_{\theta d} = \frac{2(I_p - I_r)}{L} \tau \dot{\phi}^2 \cos(\dot{\phi} t) \tag{2.11}$$

Where I_p and I_r are the polar and radial moments of inertia. The μ and τ represent the static and dynamic eccentricity values. These eccentricity forces are used to try to best represent a real-world spindle design that is not a perfect spindle. Without these forces, the spindle would not behave as it would in the real world. The moments about the x-axis and y-axis can be seen below in Equations 2.12 and 2.13. These moment equations are used to reduce the number of unknowns in the system.

$$M_x = -F_{ya}\left(\frac{L}{2}\right) + F_{yb}\left(\frac{L}{2}\right) \tag{2.12}$$

$$M_y = F_{xa}\left(\frac{L}{2}\right) - F_{xb}\left(\frac{L}{2}\right) \tag{2.13}$$

The force in these moment equations are the electromagnetic forces generated by the AMBs. Each AMB location has its own set of force equations. The electromagnetic force equations are discussed in the following section.

2.2 Electromagnetic Forces

The AMBs used for this system are a homopolar design that use coils to produce the electromagnetic force. The homopolar design of these AMBs helps reduce the eddy current effect. The radial direction force is generated by energizing coil pairs on the laminated stator [6]. These coil pairs are located 180 degrees apart with two pairs in the AMB. The force generated is added to the permanent magnetic force and the controller is able to reduce the energy in either coil depending on the needed position of the spindle. The axial force is also generated by energizing two coaxial coils that are located inside the outer edge of the AMB [6]. The axial force is also added to the permanent magnet force in the axial direction and is also able to be controlled depending on the desired position of the spindle. The permeant magnet force can be adjusted depending on the demands of the AMB. The assumptions used for the development of the AMB forces are as follows: flux leakage is negligible, fringing effect of the flux is negligible, constant permeability of the stator and rotor and the cross section is uniform along the entire magnetic loop. The equations used to represent the magnetic forces can be seen below in Equations 2.14 through 2.28 [9].

$$F_{xa} = f_{ta} - f_{ba} \tag{2.14}$$

$$F_{ya} = f_{ra} - f_{la} \tag{2.15}$$

$$F_{xb} = f_{tb} - f_{bb} \tag{2.16}$$

$$F_{yb} = f_{rb} - f_{lb} \tag{2.17}$$

$$F_{za} = f_{za1} - f_{za2} \tag{2.18}$$

$$f_{ta} = \frac{\mu_0 N_t^2 A_g (i_0 + \mu_{xa})^2}{4(C_r + x_a)^2} \tag{2.19}$$

$$f_{ba} = \frac{\mu_0 N_t^2 A_g (i_0 - \mu_{xa})^2}{4(C_r - x_a)^2} \tag{2.20}$$

$$f_{ra} = \frac{\mu_0 N_t^2 A_g \left(i_0 + \mu_{ya}\right)^2}{4(C_r + y_a)^2} \tag{2.21}$$

$$f_{la} = \frac{\mu_0 N_t^2 A_g \left(i_0 - \mu_{ya}\right)^2}{4(C_r - y_a)^2} \tag{2.22}$$

$$f_{tb} = \frac{\mu_0 N_t^2 A_g (i_0 + \mu_{xb})^2}{4(C_r + x_b)^2} \tag{2.23}$$

$$f_{bb} = \frac{\mu_0 N_t^2 A_g (i_0 - \mu_{xb})^2}{4(C_r - x_b)^2} \tag{2.24}$$

$$f_{rb} = \frac{\mu_0 N_t^2 A_g \left(i_0 + \mu_{yb}\right)^2}{4(C_r + y_b)^2} \tag{2.25}$$

$$f_{lb} = \frac{\mu_0 N_t^2 A_g \left(i_0 - \mu_{yb}\right)^2}{4(C_r - y_b)^2} \tag{2.26}$$

$$f_{za1} = \frac{\mu_0 N_t^2 A_g (i_0 + \mu_{za})^2}{4(C_r + z_a)^2} \tag{2.27}$$

$$f_{za2} = \frac{\mu_0 N_t^2 A_g (i_0 - \mu_{za})^2}{4(C_r - z_a)^2} \tag{2.28}$$

It is important to note that these equations do not have a geometric coupling factor and this is due to the design of these AMBs which do not experience geometric coupling. In the above equations μ_0 is the permeability of free space $\left(4\pi * 10^{-7} \frac{N}{A^2}\right)$, N_t is the

number of turns per coil, A_g is the area of the coil, i_0 is the current used to produce to the bias force for this system that is zero because it uses permanent magnets to produce that force, $\mu_{xa} \dots \mu_{za}$ is the control current, C_r is the nominal air gap between the stator and rotor, and $x_a \dots z_a$ are the positions of the spindle from its zero state. The positions are measured in reference to the center of gravity of the spindle. To obtain the position at the individual AMBs, the below Equations 2.29 through 2.33 are used.

$$x_a = x + \left(\frac{L}{2}\right)\sin(\theta) \tag{2.29}$$

$$x_b = x - \left(\frac{L}{2}\right)\sin(\theta) \tag{2.30}$$

$$y_a = y - \left(\frac{L}{2}\right)\sin(\psi) \tag{2.31}$$

$$y_b = y + \left(\frac{L}{2}\right)\sin(\psi) \tag{2.32}$$

$$z_a = z - \left(\frac{L}{2}\right)\sin(\theta) - \left(\frac{L}{2}\right)\sin(\psi) \tag{2.33}$$

2.3 Spindle and AMB Parameters

The constants used in the above equations are based off an existing model [3]. These constants are based on a real spindle design. Having these constants represent real values help to validate the controller design and the capability of actually controlling this system in the real world. The constant values for the spindle and AMB can be found below in Table 1 and Table 2.

Table 1: Spindle Parameters

Parameter	Symbol	Value	Unit
Length of Spindle	L	0.33	m
Mass of Spindle	m_r	13.9	kg
Static Eccentricity	μ	$1 * 10^{-5}$	m
Dynamic Eccentricity	τ	$4 * 10^{-4}$	rad
Polar Moment of Inertia	I_p	0.0134	kg * m^2
Radial Moment of Inertia	I_r	0.232	kg * m^2
Spindle Speed	$\dot{\phi}$	192,000	RPM

Table 2: AMB Parameters

Parameter	Symbol	Value	Unit
Permeability of Free Space	μ_0	$4\pi * 10^{-7}$	Henry/meter
Area of Coil	A_g	$1.532 * 10^{-3}$	m^2
Number of Turns	N_t	400	turns
Nominal Air Gap	C_r	$0.55 * 10^{-3}$	m
Bias Current	i_0	0	A

2.4 Nonlinear Time-Frequency Control

The controller used for this research is a nonlinear time-frequency controller. The controller algorithm was based on the discrete wavelet transformations (DWT) and filtered-x least-mean-square (FXLMS) algorithm [10]. The specific wavelets used for this research are the Daubechies-3 wavelets. The scaling and wavelet functions are constructed using exact filter coefficients. The coefficients used can be seen below in

Table 3 and the functions created using the coefficients are given in Figure 9 and Figure 10 [10].

Table 3: Daubechies-3 Filter Coefficients

Low-Pass Filter Coefficients	High-Pass Filter Coefficients
h_1 = 0.33267055295095688	g_1 = 0.035226291882100656
h_2 = 0.80689150931333875	g_2 = 0.085441273882241486
h_3 = 0.45987750211933132	g_3 = -0.13501102001039084
h_4 = -0.13501102001039084	g_4 = -0.45987750211933132
h_5 = -0.085441273882241486	g_5 = 0.80689150931333875
h_6 = 0.035226291882100656	g_6 = -0.33267055295095688

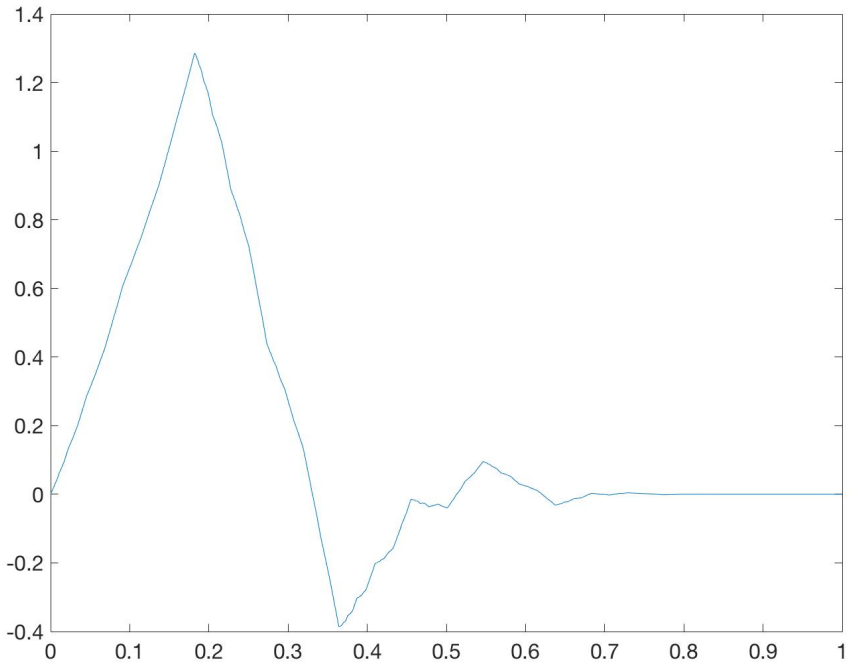

Figure 9: Scaling Function for Dauechies-3 Wavelet

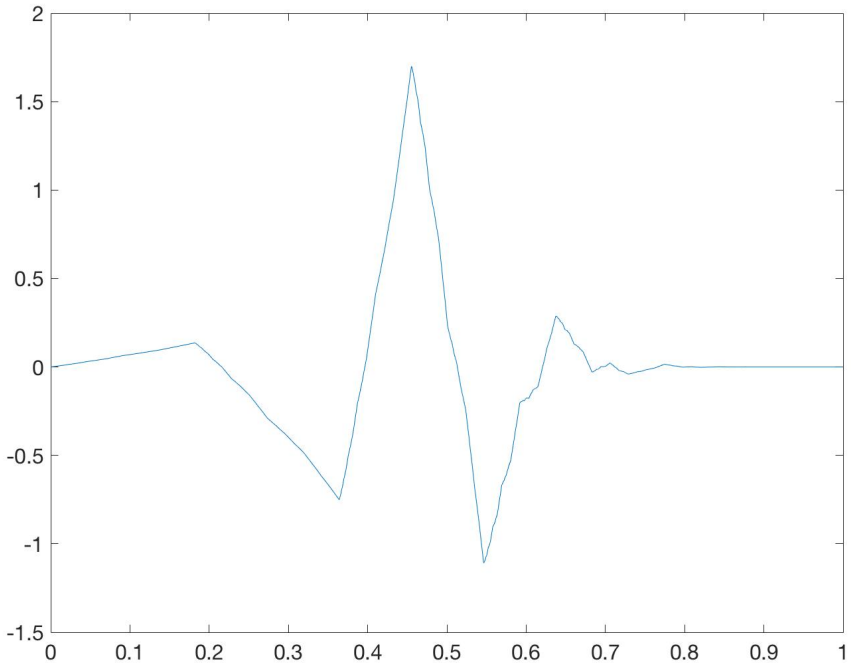

Figure 10: Wavelet Function for Dauechies-3 Wavelet

The logic of this controller implements DWT and FXLMS adaptive filters to perform a feedforward control, online identification and to construct parallel adaptive filter banks [10]. The controller uses feedforward to update the adaptive filter coefficients with the data obtained from the system error. The use of DWT allows the controller to simultaneously control time and frequency responses of the system and the transformation between the two domains is lossless. The simultaneous control of both domains is important for a high-speed spindle design.

The controller logic has two main loops. These loops are the inner and outer loops. Both of these loops are used simultaneously to bring the system online and under control. The main purpose of the inner loop is online system identification which enables the outer loop to bring the identified system to the desired position. All of this is done by using feedforward control through updating the adaptive filter coefficients. The outer loop starts by decomposing the input signal, x(n), into its wavelet coefficients using the N by N DWT matrix, T. Then the adaptive filter, W_2, takes the decomposed information and generates the controlled signal, u(n). This control signal is based on the actual error, e(n), of the system which is the difference of the desired position, d(n), from the actual position, y(n), of the system. Adaptive filter, W_2, is updated using the actual error of the system, e(n). Adaptive filter, W_1, is updated from the system identification error, f(n), which is the difference of the actual error of the system, e(n), and the predicted system error, $\bar{e}$. This process is repeated while continually updating the values of the adaptive filters by trying to minimize the error. The logic of the controller can be seen below in Figure 11.

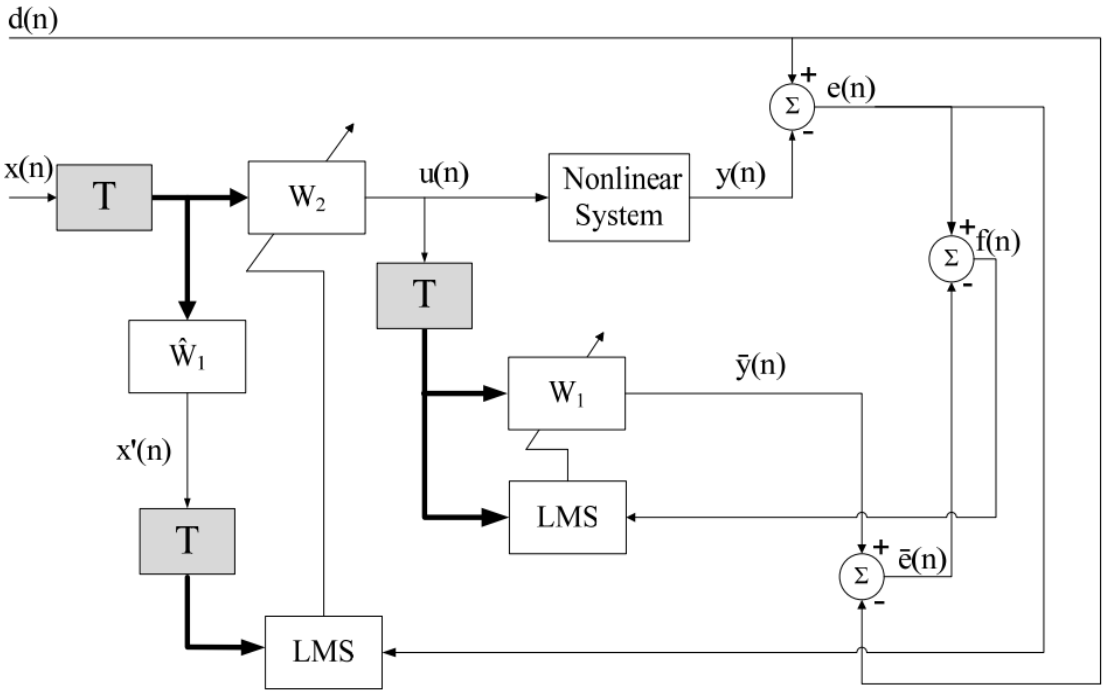

Figure 11: Logic of Nonlinear Time-Frequency Controller [10]

All of the information in this controller is stored in signal vectors of length N. The information is stored in vectors so the N by N DWT matrix, T, can be incorporated into the algorithm. These vectors are updated by adding the incoming data and dropping the last data point every iteration. The signal vectors in Equations 2.34 through 2.38 are as follows: X(n) is the input signal, U(n) is the controlled signal, X'(n) is the transformed input signal for the feedforward part of the controller, E(n) is the error signal, and F(n) is the difference of predicted and actual system error [10].

$$X(n) = [x(n) \quad x(n-1) \quad \dots \quad x(n-N+1)]^T \tag{2.34}$$

$$U(n) = [u(n) \quad u(n-1) \quad \dots \quad u(n-N+1)]^T \tag{2.35}$$

$$X'(n) = [x'(n) \quad x'(n-1) \quad \dots \quad x'(n-N+1)]^T \tag{2.36}$$

$$E(n) = [e(n) \quad e(n-1) \quad \dots \quad e(n-N+1)]^T \tag{2.37}$$

$$F(n) = [f(n) \quad f(n-1) \quad \dots \quad f(n-N+1)]^T \tag{2.38}$$

The adaptive filter coefficients are also updated and stored in a vector. The weight vector can be seen below in Equations 2.39 and 2.40 [10].

$$W_1(n) = \left[w_{1,0}(n) \quad w_{1,1}(n-1) \quad \dots \quad w_{1,N-1}(n-N+1)\right]^T \tag{2.39}$$

$$W_2(n) = \left[w_{2,0}(n) \quad w_{2,1}(n-1) \quad \dots \quad w_{2,N-1}(n-N+1)\right]^T \tag{2.40}$$

The predicted system error can be calculated using Equation 2.41 [10]. This is calculated using the desired position and the predicted system position.

$$\bar{e}(n) = d(n) - \bar{y}(n) \tag{2.41}$$

The predicted system position can be calculated using Equation 2.42 where W_1 is an adaptive filter, and T is the DWT matrix, and U(n) is the control signal vector [10].

$$\bar{y}(n) = W_1^T(n)TU(n) \tag{2.42}$$

The actual system error can be calculated using Equation 2.43 [10]. This is calculated using the desired position and the actual position.

$$e(n) = d(n) - y(n) \tag{2.43}$$

The difference between the actual and predicted system error can be represented as [10].

$$f(n) = e(n) - \bar{e}(n) \tag{2.44}$$

The least-mean-square algorithm used to update the adaptive filters can be seen below in Equations 2.45 and 2.46 [10]. With μ_1 and μ_2 being the optimization step sizes that are user defined.

$$W_1(n+1) = W_1(n) - \mu_1 TU(n)f(n) \tag{2.45}$$

$$W_2(n+1) = W_2(n) + \mu_2 TX'(n)e(n) \tag{2.46}$$

The transformed input signal, x'(n), can be seen below in Equation 2.47 [10].

$$x'(n) = W_1^T(n)TX(n) \tag{2.47}$$

This is used to update the, X'(n), signal vector which will be used to update the, W_2, the adaptive filter bank.

3. RESULTS AND DISCUSSION

The high-speed spindle and AMB design are programmed in a Matlab/Simulink environment. For this simulation, a driving frequency of 3,200 Hz and an integration time step of $1x10^{-5}$ seconds are used. This time step allowed for the detection of frequencies up to 50 kHz. The time step is verified to be correct by using convergence study before proceeding with testing the system. Also during the simulations an impulse force is used after the system had reached a controlled state. This impulse force is used to demonstrate the robustness of the controller and its abilities to regain control of the system after a large impulse force is exerted. The impulse force used in the x-axis and y-axis is 500 kN in magnitude and the force in the z-axis is 250 kN in magnitude. The force is applied at all the axes at the same time. The impulse force is applied at t = 0.3 seconds during the simulation. Both the x-axis and z-axis have the force applied in the positive direction and the y-axis has the force applied in the negative direction. This impulse force is applied over a time frame of one thousandth of a second. With such a large force over a short time period it could have caused the system to enter chaotic state. Also, to better represent a real world shaft a static eccentricity is used to create an imperfect shaft. This static eccentricity value is $1.0x10^{-5}$ meters. The shaft is also considered flexible so as to lead to whirling and more nonlinearities being introduced into the system. Whirling occurs when the system reaches a speed that induces excessive vibrations in the system. The assumptions used for the development of the AMB forces are as follows: flux leakage is negligible, fringing effect of the flux is negligible, constant permeability of the stator and rotor and the cross section is uniform along the

entire magnetic loop. The following sections presents the data obtained from the simulations for the time and frequency domain.

3.1 Time Domain Results

The time domain results in this section represent the displacement of the spindle. These displacements are generated by driving the system at an operational speed of 192,000 RPMs. At this speed, the whirling of the flexible shaft becomes a major driving force for unwanted vibrations in the system. These vibrations could lead to system failure. The type of failure that could occur in this system is an excessive amount of displacement due to the vibrations. The displacement can cause the spindle to hit the AMBs and result in a total system failure. If the AMBs fail, the spindle will no longer be supported by the electromagnetic force that is keeping the system under control. The maximum displacement the spindle can undergo before hitting the AMBs in the x-direction is the nominal air gap value of 0.55×10^{-3} meters. The maximum displacement the spindle moves in the x-direction is during the impulse force. This force of 500 kN is representing an object striking the spindle during operation. The force moves the spindle 1.07×10^{-4} meters which is less than a fifth of the maximum displacement allowed. This amount of movement is considered acceptable for the system. During the initial stages of the simulation when the controller is still trying to bring the system under control it experiences a smaller displacement value than that of the impulse force. The initial displacement value is 8.70×10^{-5} meters which is also less than a fifth of the maximum displacement allowed. This initial displacement is also considered an acceptable amount for the system. Once the controller is able to control the system the displacement of the

spindle is greatly reduced. The controlled displacement of the spindle is 2.85×10^{-5} meters which is slightly more than a twentieth of the maximum displacement allowed. This demonstrates how capable the controller is in bringing the system under control. The displacements at bearing A and B are the same because of the symmetry of the system. The spindle displacement for bearing A and B at a velocity of 192,000 RPMs can be seen below in Figure 12 and Figure 13. Also, the summarized displacement data for the x-direction are given in Table 4.

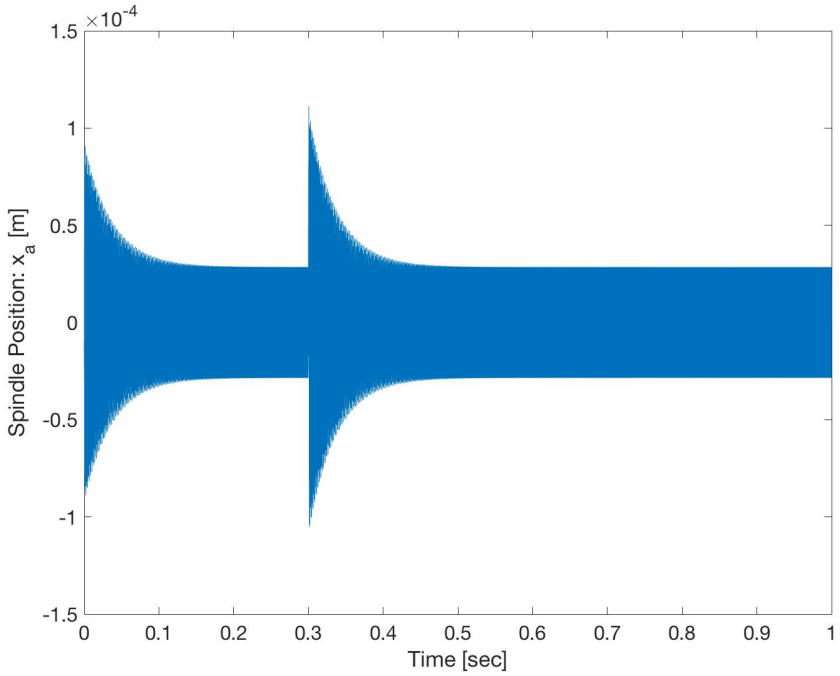

Figure 12: Spindle Position X_a at 192,000 RPM

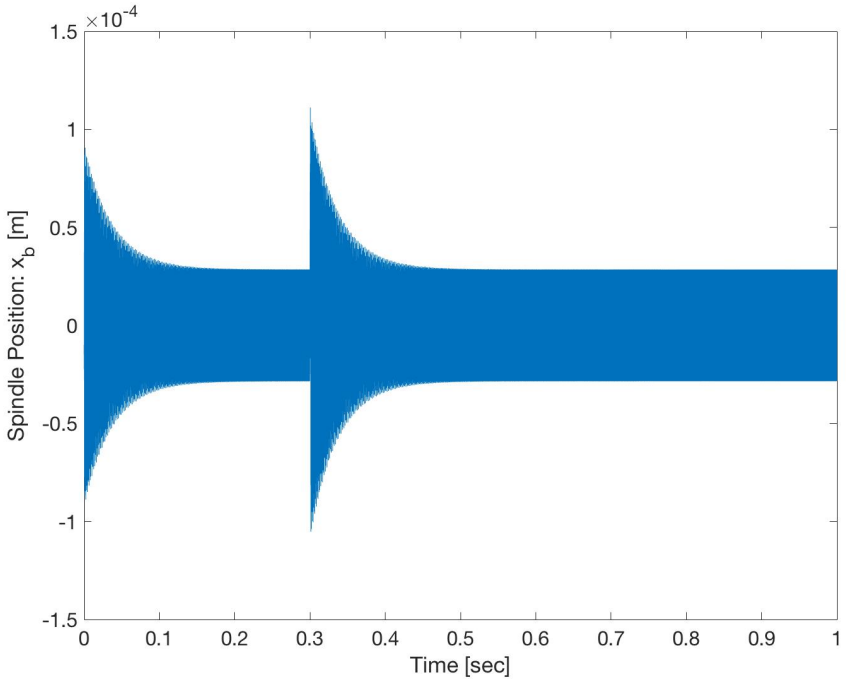

Figure 13: Spindle Position X_b at 192,000 RPMs

Table 4: X-Direction Displacements of Spindle

	Displacement (meters)	**Percentage of Air Gap (%)**
Initial Displacement	$8.70 * 10^{-5}$	15.8
Impulse Displacement	$1.07 * 10^{-4}$	19.5
Controlled Displacement	$2.85 * 10^{-5}$	5.2

The maximum displacement in the y-direction is the same nominal air gap value of $0.55x10^{-3}$ meters used in the x-direction. The difference for the y-direction displacements is the maximum displacement occurred at the start of the system. Not

when the impulse force is applied to the spindle. The initial displacement is due to the acceleration of the spindle. This acceleration is caused by the eccentricities of the flexible shaft. The initial startup displacement of the spindle is 1.21×10^{-4} meters which is less than a quarter of the maximum displacement allowed. This displacement value is still considered acceptable for the system. The next largest displacement is caused by the impulse force at t = 0.3 seconds during the simulation. However, this impulse force is applied in the negative y-direction with a force of 500 kN. This force was applied at the same time as the positive x-direction impulse force. The displacement value caused by the impulse force is 9.38×10^{-5} which is less than a fifth of the maximum displacement allowed. Since this displacement is less than the startup displacement it is also considered acceptable. Also, just like in the x-direction when the controller gained control of the system it is able to reduce the maximum displacement seen in the y-direction of the system. The controlled displacement value is 2.21×10^{-5} meters which is a less than a twentieth of the maximum displacement allowed. This demonstrates how capable the controller is in bringing the system under control in both the x-direction and y-direction. The displacements at bearing A and B are the same because of the symmetry of the system. The spindle displacement for bearing A and B at a velocity of 192,000 RPMs can be seen below in Figure 14 and Figure 15. Also, the summarized displacement data for the y-direction are given in Table 5.

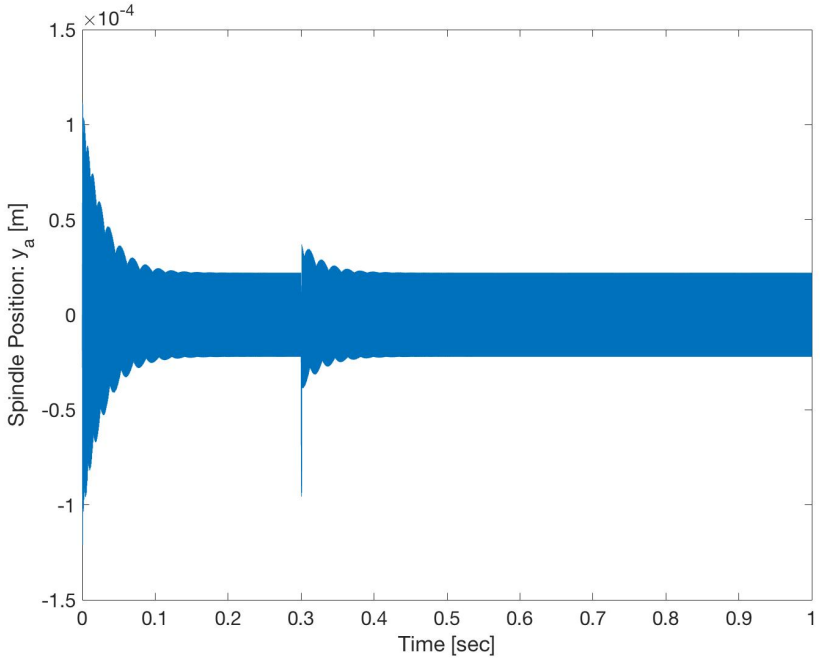

Figure 14: Spindle Position Y_a at 192,000 RPMs

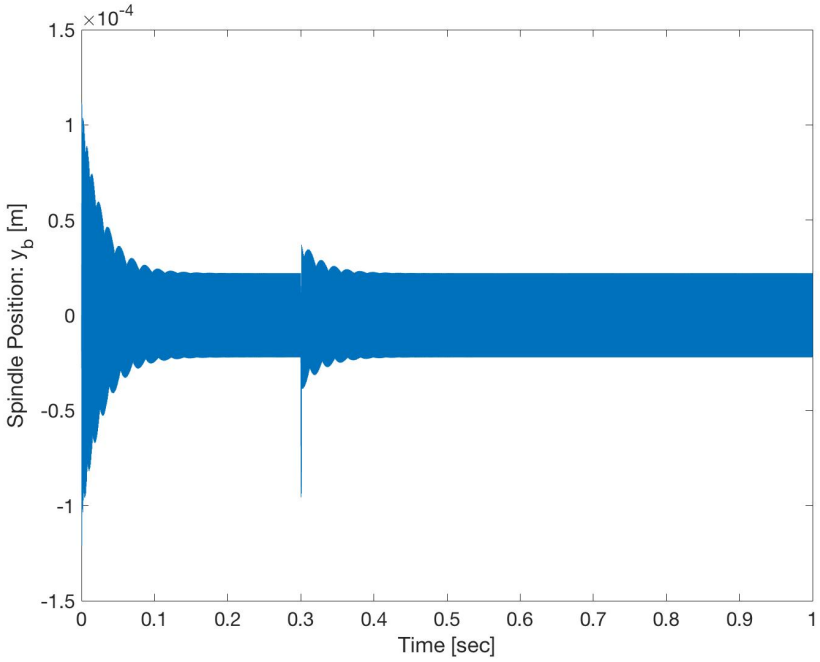

Figure 15: Spindle Position Y_b at 192,000 RPMs

Table 5: Y-Direction Displacements of Spindle

	Displacement (meters)	Percentage of Air Gap (%)
Initial Displacement	$1.21 * 10^{-4}$	22.0
Impulse Displacement	$9.38 * 10^{-5}$	17.1
Controlled Displacement	$2.21 * 10^{-5}$	4.0

The maximum displacement in the z-direction is the same nominal air gap value of $0.55x10^{-3}$ meters used for the x-direction and y-direction. The difference in the z-direction from the other directions is the initial displacement value is user determined. This initial displacement is used to represent a spindle that is not perfectly aligned in the z-direction at the beginning of the simulation. The initial displacement has to be set because the shaft has no acceleration or velocity in the z-direction at time zero. The initial displacement value is $1.0x10^{-4}$ meters which is a little less than a twentieth of the maximum displacement allowed. This displacement is considered to be an acceptable amount for the needed representation of misalignment in the simulation. The impulse force for the z-direction is applied in the positive direction with a force of 250 kN. This force is also applied at the same time when all the other impulse forces are applied. The displacement caused by this impulse force is $8.16x10^{-5}$ meters which is less than a fifth of the maximum displacement allowed. This amount of displacement is considered acceptable. The displacement for the controlled z-direction is significantly smaller than all the other controlled directions because no imbalances are introduced in the spindle in

the z-direction. As the controller brings the z-direction under control, the displacement value in that direction will go to zero. This shows how well the controller is able to handle a system with no imbalances. Also, the controller is capable of reaching a zero state and staying there without continually oscillating around that value. Only bearing A has z-direction displacement because it is the only bearing that has the thrust component. The spindle displacement for bearing A at a velocity of 192,000 RPMs can be seen below in Figure 16. Also, the summarized displacement data for the z-direction are given in Table 6.

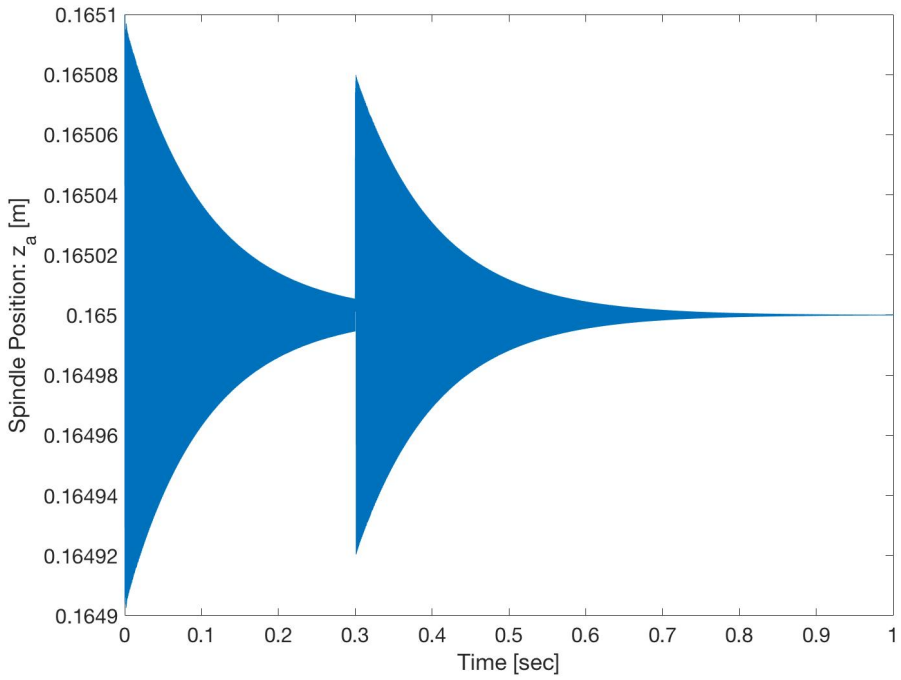

Figure 16: Spindle Position Z_a at 192,000 RPMs

Table 6: Z-Direction Displacements of Spindle

	Displacement (meters)	Percentage of Air Gap (%)
Initial Displacement	$1.0 * 10^{-4}$	18.2
Impulse Displacement	$8.16 * 10^{-5}$	14.8
Controlled Displacement	0	0

3.2 Frequency Domain Results

To further validate the robustness of the controller design, the controlled response of the system is transformed from the time domain to the frequency domain. This is done to show that the controller can simultaneously control the time and frequency domain. Many controllers can only control the time domain and that it is a mistake to assume if the time domain is controlled then the system is controlled. For a system to be truly controlled both the time and frequency domains need to be under control. The method used to transform the time domain information to the frequency domain is the Hilbert-Huang Transform (HHT). The HHT does not use a set of predetermined basis functions like the Fourier-based methods do. The HHT is a two-part process. The first part uses empirical mode decomposition (EMD) and the second part uses Hilbert spectral analysis. The HHT method has better temporal and frequency resolutions when compared to Fourier-based methods [11]. EMD is locally adaptive and suitable for analysis of nonlinear or nonstationary systems [11]. EMD starts by examining signals at their local level of oscillations. This decomposition technique

extracts a finite number of functions that are called intrinsic mode functions (IMFs). The IMFs are obtained using an algorithm called the shifting process. This process is based on two constraints that each mode has the same number of zero crossings and extrema and also has symmetric envelopes defined by the local maxima and minima [11]. Also, EMD assumes that the input signal has at least two extrema. The shifting process generates a finite number of IMFs that are orthogonal [11]. The first IMF contains the highest frequency information. As the decomposition continues each IMF after has a lower frequency than the previous IMF. Once all the IMFs are found the Hilbert spectral analysis can be used to create the corresponding monocomponent analytic signals and these obtained signals can then be used to determine the signals instantaneous frequencies and amplitude modulations [10]. The following instantaneous frequency information is for the x-direction and y-direction because these directions had the major nonlinearities in their frequency. The z-direction only has one frequency but it is mitigated as the system is brought to the desired location. The x-direction and y-direction have three major modes of frequencies. These major modes are discussed below.

In the x-direction, the first major mode is caused by the driving frequency mode of 3,200 Hz. This driving frequency causes the system to enter a highly broadband state with frequencies ranging from 8,602 Hz to 723 Hz. This broadband state demonstrates how nonlinear the system response is. If this system is left in this state of broadband it would lead to a system failure even if the system is controlled in the time domain. Once, the controller brings the first mode under control it is able reduce the bandwidth of the

system down to a frequency range of 3,274 Hz to 3,153 Hz. The first major mode can be seen below in Figure 17.

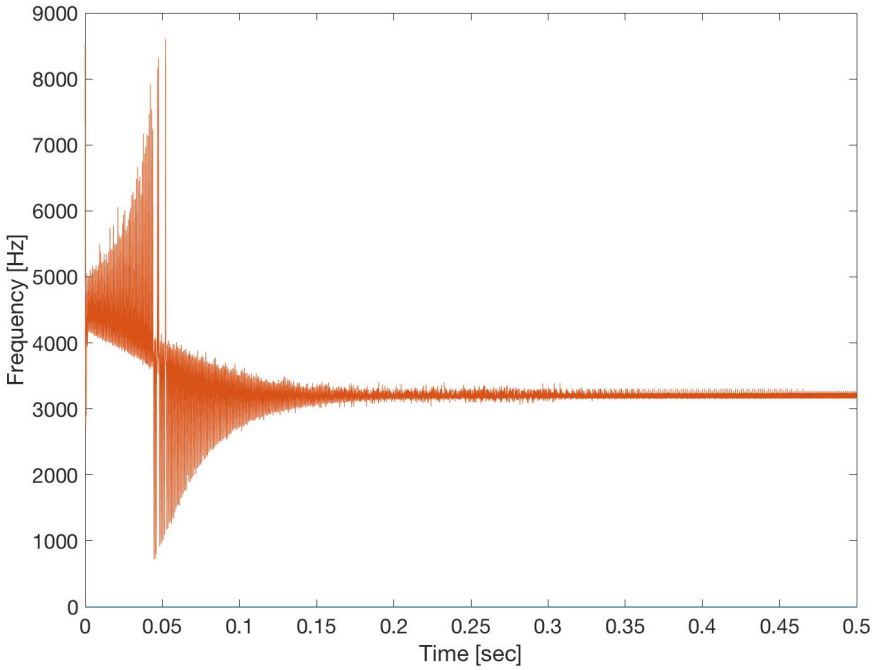

Figure 17: First Major Mode of Frequency for X-Axis

The second major mode of the system is also a broadband response but this response is not as broadband as the first mode. The range of this frequency response is 3,870 Hz to 22 Hz. Once, the controller gained control of the system it is able to reduce the bandwidth of the system to a frequency range of 1,821 Hz to 1,440 Hz. The second major mode can be seen below in Figure 18.

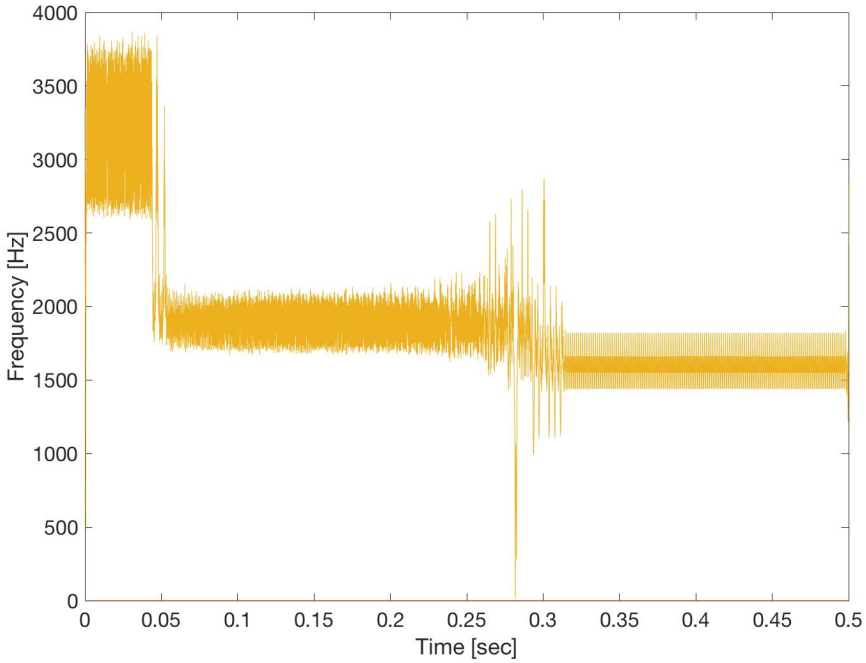

Figure 18: Second Major Mode of Frequency for X-Axis

The third major mode of the system is also a broadband response but this response is not as broadband as the first mode. The range of this frequency response is 2,276 Hz to 108 Hz. Once, the controller gained control of the system it is able to reduce the bandwidth of the system to a frequency range of 840 Hz to 752 Hz. The third major mode can be seen below in Figure 19.

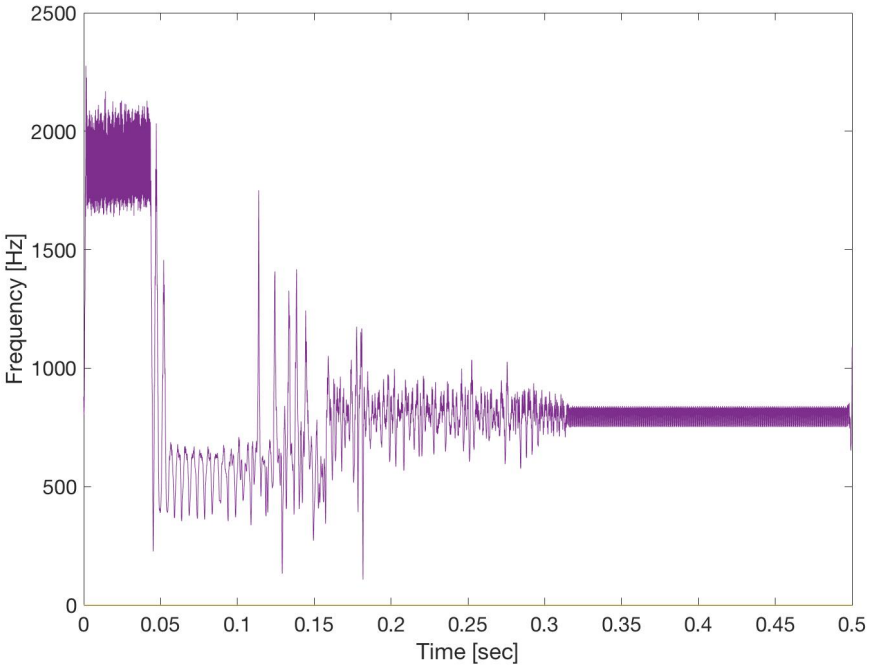

Figure 19: Third Major Mode of Frequency for X-Axis

All three major modes and how they interact can be seen below in Figure 20. This instantaneous frequency response demonstrates the robustness of the controller. The controller is capable of bringing a highly nonlinear and broadband system response to a quasi-periodic response. With a quasi-periodic response, the nonlinear system is now a predictable system.

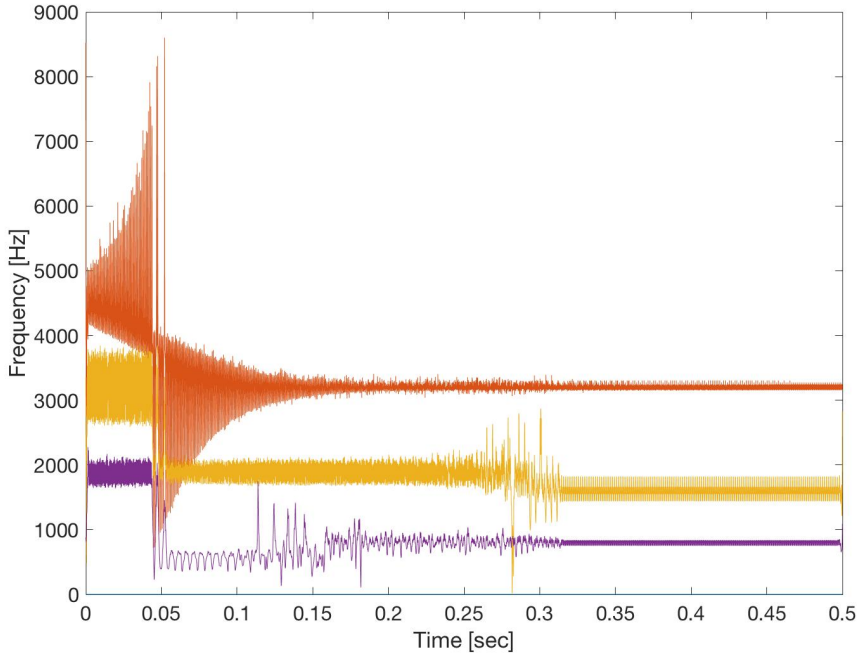

Figure 20: Instantaneous Frequency Response of X-Axis at 192,000 RPMs

In the y-direction, the first major mode is caused by the driving frequency of 3,200 Hz. This driving frequency also causes the system to enter a highly broadband state just as it experienced in the x-direction. The frequencies ranged from 7,811 Hz to 680 Hz. The y-direction is not as broadband as the x-direction but the system is still highly nonlinear and if left uncontrolled would lead to the failure of the system. Once the controller is able to gain control of the system it reduces the bandwidth of the frequency. The controlled frequency range is 3,327 Hz to 3,139 Hz. The first major mode can be seen below in Figure 21.

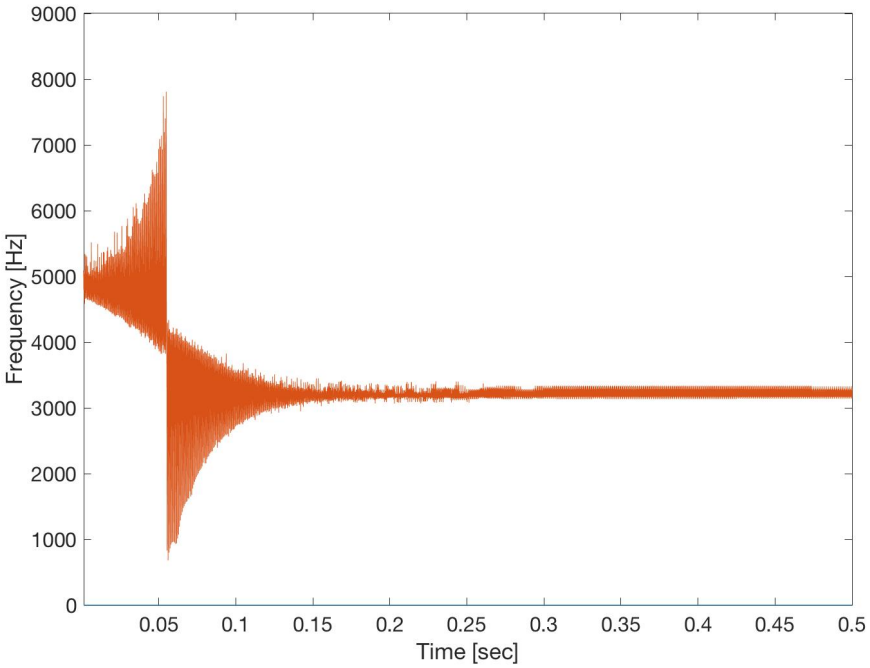

Figure 21: First Major Mode of Frequency for Y-Axis

The second major mode is also a broadband response but not as broadband as the first major mode. The frequency range of this mode is 3,831 Hz to 2 Hz. Once, the controller is able to bring the system under controlled it is able to reduce the bandwidth of the system. The controlled frequency range is 1,891 Hz to 1,402 Hz. The second major mode can be seen below in Figure 22.

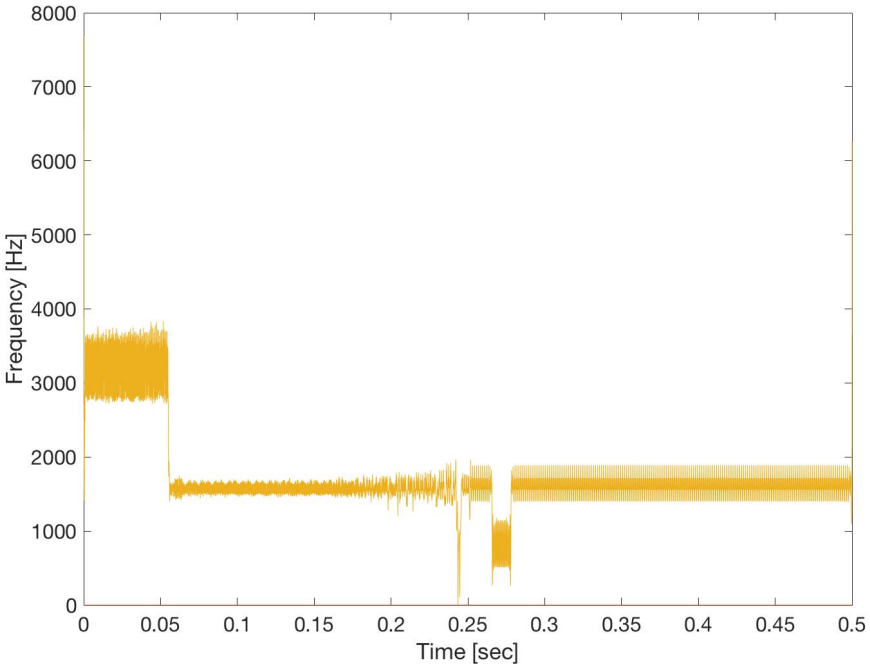

Figure 22: Second Major Mode of Frequency for Y-Axis

The third major mode is also a broadband frequency response because of a major spike at the time 0.27 seconds. This response is broader than that of the second major mode. The frequency range of this mode is 4,824 Hz to 38 Hz. Even with this major spike the controller is still able to bring the system under control. The controlled frequency range is 842 Hz to 762 Hz. The third major mode can be seen below in Figure 23.

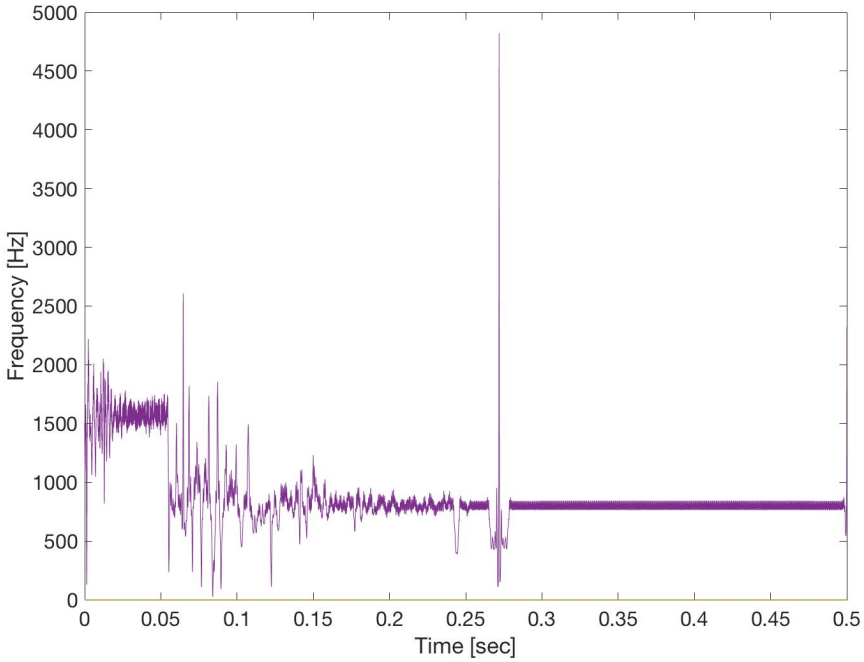

Figure 23: Third Major Mode of Frequency for Y-Axis

All three major modes and how they interact can be seen below in Figure 24. The controller is also able to bring the y-direction under control. The controller reduces the highly nonlinear and broadband response to a quasi-periodic and predictable response. This demonstrates the robustness of the controller.

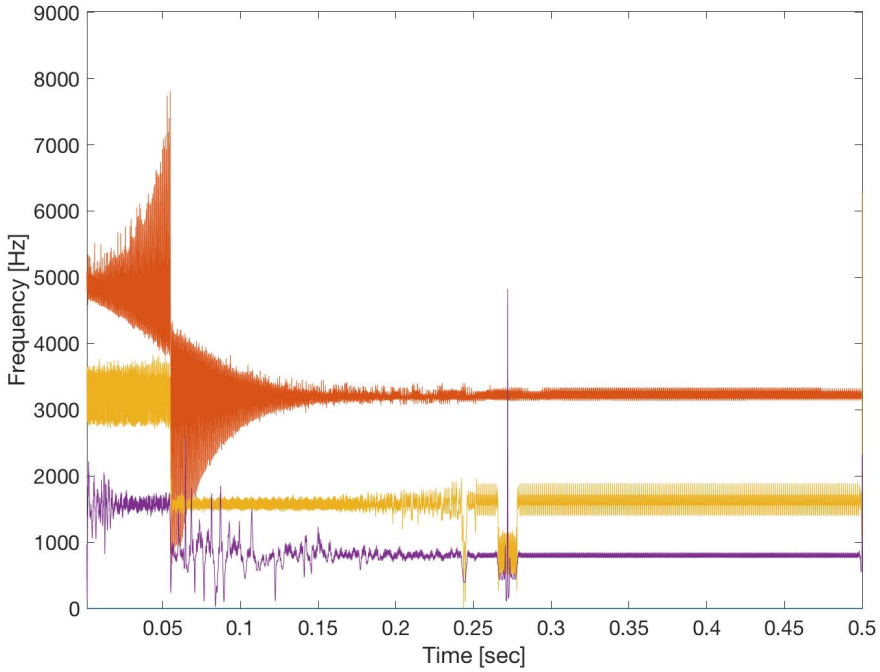

Figure 24: Instantaneous Frequency Response of Y-Axis at 192,000 RPMs

In these simulations as the time progresses, the controller is continually decreasing the bandwidth of the frequency response. If the controller is given enough time without outside perturbation introduced into the system then the bandwidth of the modes will continue to reduce. But in real applications the system will always have some outside perturbation and the controller will be capable of reducing the bandwidths and bringing the system to a predictable quasi-periodic state. The summarized bandwidths for the system response are given in Table 7.

Table 7: Summarized Frequency Bandwidths

	Major Mode	Maximum Bandwidth [Hz]	Controlled Bandwidth [Hz]	Percent Remaining [%]
X-Axis	1	7879	121	1.5
	2	3848	381	9.9
	3	2168	88	4.1
Y-Axis	1	7131	188	2.6
	2	3829	489	12.8
	3	4786	80	1.7

4. CONCLUSIONS AND FUTURE WORKS

The nonlinear time-frequency controller was demonstrated to be able to control a high-speed spindle in all the axes using active magnetic bearings in both the time and frequency domain simultaneously. These AMBs were tested to demonstrate the capability of a new bearing design that was different than the conventional AMB design. With these AMBs, the overall weight of the system will be reduced and the number of AMBs needed for stable control will also be reduced from three to two. Also with these bearings the need for a backup bearing will no longer be required because of the permanent magnetics used to levitate the shaft. This permanent magnet system will also allow the system to operate on less power than a conventional AMB performing the same task.

The design of this system was shown to be able to operate at speeds up to 192,000 RPMs using combination bearings. During the controlled stage of operation, the spindle was only allowed to move 2.85×10^{-5} meters in the x-direction, 2.21×10^{-5} meters in the y-direction and the z-direction was approaching zero displacement from the desired location. The controller was proven capable of handling an impulse force added to the already controlled system. When the force excited the controlled system, the controller was able to bring the system back under control in 0.2 seconds. However, when the impulse force perturbed the system the controller immediately began bring the system back under control and to the desired position.

The controller was also capable of controlling the frequency domain simultaneously with the time domain. The system responded with a highly nonlinear

broadband frequency response when it was excited with the driving frequency of 3,200 Hz. This broadband response ranged from 2 Hz to 8,602 Hz. Even though the systems response was broadband the controller was able to reduce the bandwidth of the response down to 1.5% of the original bandwidth. This capability to reduce the bandwidth and bring the system into a quasiperiodic state demonstrates the robustness of the controller.

Overall this high-speed spindle design demonstrated the capability of running and being controlled at a speed of 192,000 RPMs without the need of backup bearings. However, the system needs further investigation. The next step in the endeavor of this research would be to physically validate the AMBs and demonstrate that the controller can bring the spindle to a stable state in both the time and frequency domain. The system would be tested at lower speeds at first to validate the stability of the controller before proceeding to reach the speeds obtained in this research. To test the system at low speeds the spindle can be driven with an electric motor to validate the stability of the system. Once stability is verified the system could then be pushed further and the true maximum speed of the physical system could be discovered. Reaching speed of 192,000 RPMs will require other methods of driving the system. Some of the possible ways that have been researched are driving the system with another AMB. With this AMB driving the system no physical contact with the spindle and driving force would made. This method would reduce the amount of outside perturbations. However, validating the physical system would be a major step forward in this research even if at a speed lower than stated in this research.

REFERENCES

[1] 2012, "Shamrock Machinery Company," from https://www.shamrockmachinery.com/wp-content/uploads/2017/02/HR-26-ROUGHNECK-lathe-technical-offer.pdf

[2] Schweitzer, G., 2009, "Applications and Research Topics for Active Magnetic Bearings," ETH Zurich, Switzerland.

[3] Liu, M., 2015, "Investigation on the Applicability of Active Magnetic Bearings to High Speed Spindle Design," M.S. Thesis, Texas A&M University, College Station, TX.

[4] Filatov, A., and Hawkins, L., 2013, "General Explanation of How Magnetic Bearings Work," Clanetix Technologies LLC, Cerritos, CA.

[5] Knospe, C. R., and Zhu, L., 2011, "Performance Limitations of Non-Laminated Magnetic Suspension Systems," IEEE Transactions on Control Systems Technology, 19(2), pp. 327-336.

[6] McMullen, P. T., Huynh, C. S., and Hayes, R. J., 2000, "Combination Radial-Axial Magnetic Bearing," Seventh International Symp. on Magnetic Bearings, pp. 473-478.

[7] Ji, J. C., Hansen, C. H., and Zander, A. C., 2008, "Nonlinear Dynamics of Magnetic Bearing Systems," Journal of Intelligent Material Systems and Structures, 19, pp. 1471-1491.

[8] Jeon, H. W., and Lee, C. W., 2013, "Proportional-Integral-Derivative Control of Rigid Rotor-Active Magnetic Bearing System via Eigenvalue Assignment for

Decoupled Translational and Conical Modes," Journal of Vibration and Control, pp. 1-22.

[9] Lewallen, C., 2016, "Novel Active Magnetic Bearing Control for a High-Speed Flywheel," M. S. Thesis, Texas A&M University, College Station, TX.

[10] Suh, C. S., and Liu, M. K., 2013, *Control of Cutting Vibration and Machining Instability: A Time-Frequency Approach for Precision, Micro, and Nano Machining*, John Wiley & Sons, College Station, TX, USA, pp. 110-164, Chap. 5-7.

[11] Nunes, J. C., and Delechelle, E., 2009, "Empirical Mode Decomposition: Applications on Signal and Image Processing," Advances in Adaptive Data Analysis, 1(1), pp. 125-175.